Transcription activator structure reveals redox control of a replication initiation reaction[†]

Cyril M. Sanders[1],*, Dmytro Sizov[2], Philippa R. Seavers[2], Miguel Ortiz-Lombardía[2] and Alfred A. Antson[2]

[1]Institute for Cancer Studies, University of Sheffield, Beech Hill Rd, Sheffield, S10 2RX, UK and [2]York Structural Biology Laboratory, Department of Chemistry, University of York, Heslington, York, YO10 5YW, UK

ABSTRACT

Redox changes are one of the factors that influence cell-cycle progression and that control the processes of cellular proliferation, differentiation, senescence and apoptosis. Proteins regulated through redox-sensitive cysteines have been characterized but specific 'sulphydryl switches' in replication proteins remain to be identified. In bovine papillomavirus type-1, DNA replication begins when the viral transcription factor E2 recruits the viral initiator protein E1 to the origin of DNA replication (*ori*). Here we show that a novel dimerization interface in the E2 transcription activation domain is stabilized by a disulphide bond. Oxidative cross-linking via Cys57 sequesters the interaction surface between E1 and E2, preventing pre-initiation and replication initiation complex formation. Our data demonstrate that as well as a mechanism for regulating DNA binding, redox reactions can control replication by modulating the tertiary structure of critical protein factors using a specific redox sensor.

INTRODUCTION

The papillomaviruses (PVs) are small DNA viruses that infect epithelial cells and cause warts, but some viruses are linked to cancers in humans (1). PVs are also important model organisms for gene control and replication in mammalian cells, as their genomes are regulated similarly. The viral transcription factor E2 is the master regulator of the PV chromosome, controlling both transcription and replication. Tethering E2 to DNA via the C-terminal DNA binding and dimerization domain (DBD) is essential for both these functions, and the N-terminal trans-activation domain (TAD) is linked to the DBD via a flexible hinge (2). The role of E2 in replication is to recruit the viral initiator protein E1 to the viral origin of replication (3; see Figure 1A). The critical E2 TAD-E1 helicase domain interaction (4,5) is conserved in bovine papillomavirus (BPV) and human papillomaviruses (HPV), and its molecular details have been revealed in the crystal structure of HPV 18 E1 in complex with the E2 TAD (6). The molecular events of the initiation of viral replication are becoming increasingly well understood. The first step in replication is the formation of an E1E2–*ori* complex on the E1 binding site (BS) and E2 BS12 (Figure 1A). This pre-initiation complex contains a dimer of E1 and a dimer of E2 (7). In a reaction that requires ATP, E2 is displaced and more molecules of E1 are recruited to *ori*. This initial E1–*ori* complex forms the nucleus of a higher order E1 initiator complex that melts the *ori* DNA. The action of the distal E2 BS11 is to promote further recruitment of E1 molecules to the precursor of the *ori*-melting complex, but E2 itself is not required directly for *ori*-melting activity (8,9). *Ori* templates with only a distal E2 binding site also support plasmid replication. *In vitro*, the initial recruitment of E1 to *ori* is also via an E1E2–*ori*-like complex, mediated exclusively through the E2 TAD-E1 helicase domain interaction, but this complex forms less efficient compared to templates with proximal E2 BS12 (10). Despite the emerging details of initiator complex assembly, the underlying mechanisms of cell-cycle regulation of BPV replication initiation remain unclear.

---

*To whom correspondence should be addressed. Tel: +44-114-271-2482; Fax: +44-114-271-3892; Email: c.m.sanders@sheffield.ac.uk
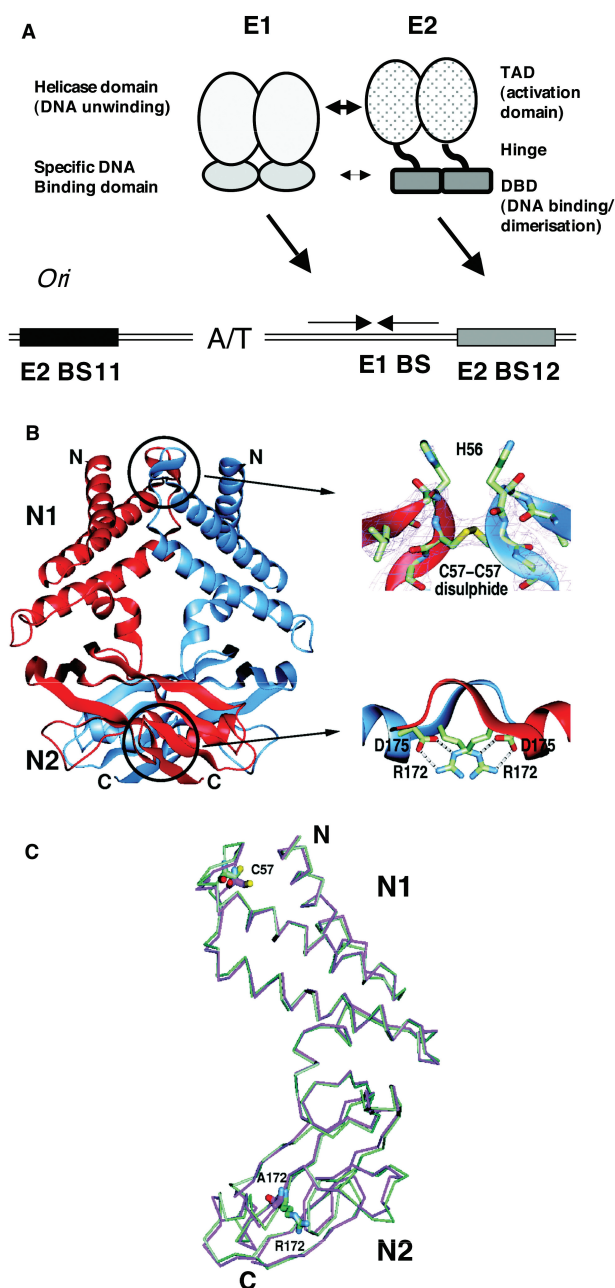
Present address:
Dmytro Sizov, Taras Shevchenko Kiev State University, Biology Faculty, Virology Department, Glushkova Ave. 2, 03127 Kiev, Ukraine.
Present address:
Miguel Oritz-Lombardía, Centro Nacional de Investigaciones Oncológicas, Programa de Biología Estructural y Biocomputación, C. Melchor Fernández Almagro 3, Madrid 28029, Spain.

Figure 1. Schematic of the BPV-1 initiator system and crystallographic results. (**A**) E1 and E2 dimers bind cooperatively to adjacent sites in *ori*, principally through an E1 helicase domain-E2 TAD interaction, but there is also a specific requirement for a weaker interaction between the DBDs of both proteins (7). The action of E2 BS11 is to promote recruitment of further E1 molecules to an initial E1–*ori* complex that form on displacement of E2 from E1E2–*ori*. A/T indicates the position of the A/T-rich region. (**B**) Ribbon diagram of the E2 TAD dimer with two monomers in different colours and the two areas of inter-subunit interactions circled and shown in detail on the right. In N1 (top right) an inter-subunit disulphide bond forms between the N-terminal α-helical domains of the TAD; critical amino acids are shown with corresponding electron density calculated at 1σ level with likelihood-weighted $2|F_o| - |F_c|$ coefficients. In N2 (bottom right), R172 and D175 residues form an ion pair interaction between the C-terminal β-sheet domains. (**C**) Superposition of wild-type (cyan) and R172A mutant (magenta) structures shown as Cα models in the same view as the blue subunit in Figure 1B. C57 and R172 are coloured according to atom type, with oxygens in red, nitrogens in blue and carbons in cyan (wild type) or magenta (R172A).

One important general question is how differential control of processes like transcription or replication is achieved by a limited array of regulatory proteins. This is particularly relevant in BPV where a single protein, E2, governs the entire genome. One mechanism is to regulate DNA-binding site occupancy, for example by DNA sequence affinity. However, controlling protein activity through redox sensitive thiols in DNA-binding domains (DBDs) has also emerged as a fundamental mechanism of regulation. Transcription factors whose DNA-binding domains are known to be regulated by thiols include AP-1, NF-kB, SP-1 but also the papillomavirus E2 DBD (11–14). In the case of E2, Cys340 has been identified as the critical residue, sensitive to oxidizing agents and sulphydryl modifying reagents such as *N*-ethylmaleimide. However, as in most cases, the underlying mechanisms of redox regulation, in particular the chemical species involved, are not known in molecular detail (14). At the same time, many cellular processes, including proliferation, differentiation, senescence and apoptosis, are redox-regulated, and proteins other than transcription factors have functional thiols (15–20). Here we describe the crystal structure of the BPV E2 N-terminal TAD where we were surprised to find a novel dimerization interface stabilized by a disulphide bond. Our complementary studies show that this interface forms between TADs within a preformed E2 dimer which is itself stabilized by a tight interaction between the C-terminal DBD domains (21). We also demonstrate that TAD–TAD dimerization inhibits the TAD–E1 interaction, in agreement with the observation that the TAD–TAD dimerization interface buries part of the surface involved in the interaction with E1. Taken together, the data suggest that in the case of BPV the E2 TAD interaction with E1 is redox regulated. Furthermore, the reactive Cys57 residue of the TAD is more sensitive to oxidation than Cys340 that regulates DNA-binding activity, indicating that the TAD dimerization reaction is a significant means of regulating BPV E2 activity. To our knowledge, this is the first demonstration that the association of activation domains with their targets can be redox regulated, and evidence supporting the hypothesis that mammalian DNA replication may come under redox control.

MATERIALS AND METHODS

Protein expression and purification

A truncated form of BPV-1 E2 comprising the N-terminal transactivation domain (TAD; amino acids 1–209 of 410) was expressed using pET11c in *Escherichia coli* BL21 (DE3). This construct includes the entire TAD, and terminates at the beginning of the E2 hinge region. Growth and expression was at 18°C for 8 h after reaching an OD_{600} ∼0.8. Frozen cells were lysed in 50 mM Tris–HCl pH 8.0 (4°C), 0.2 M NaCl, 5 mM EDTA, 20% w/v sucrose, 10 mM DTT and 1 mM PMSF by lysozyme treatment (0.5 μg ml^{-1}), and sonication. The cleared lysates were adjusted to 0.6 M NaCl, nucleic acids removed with polyethylenamine P, and protein precipitated with 30% w/v $(NH_4)_2SO_4$. The TAD was purified

by gel filtration (Sephacryl S-100, 25 mM Tris–HCl pH 8.0 (4°C), 0.25 M NaCl, 0.1 mM EDTA, 5% v/v glycerol, 2 mM DTT and 0.1 mM PMSF), anion exchange [Source Q, 0–0.25 M NaCl in 25 mM Tris–HCl pH 8.9 (4°C), 0.1 mM EDTA, 2.5 mM DTT, 10% v/v glycerol and 0.1 mM PMSF] and hydrophobic interaction chromatography [Source-phenyl, 1.25–0.25 M $(NH_4)_2SO_4$ in 25 mM NaPhosphate pH 7.5, 0.1 mM EDTA, 2 mM DTT, 10% v/v glycerol and 0.1 mM PMSF]. The purified E2 TAD was dialysed against 20 mM Tris–HCl pH 8.0 (4°C), 0.3 M NaCl, 0.15 mM EDTA, 10% v/v glycerol, 2 mM DTT and 0.1 mM PMSF, concentrated and stored at −80°C. E2 and GCN4E2 proteins were purified as previously described (22), except for an additional gel filtration step with 1 or 10 mM DTT. Mutations in the TAD were generated by overlapping primer extension.

Structure determination

Crystals were grown using hanging drop vapour diffusion by mixing 1 μl of 15 mg ml^{-1} protein solution, containing 10 mM Tris–HCl pH 8.5 and 0.3 M NaCl, with 1 μl of precipitant containing 0.1 M Tris–HCl pH 8.5, 0.3 M NaCl and 18–22% tertiary butanol. For R172A the reservoir also contained 2 mM DTT. Crystals of both wild-type and R172A mutant were transferred into a cryoprotectant solution containing 60% *tert*-butanol, 0.3 M NaCl and 10 mM Tris pH 8.5. The X-ray data were collected at ESRF and processed using DENZO and SCALEPACK (23). Crystallographic calculations were performed using the CCP4 suite of programs (24). The initial structure (wild-type protein) was solved by molecular replacement using the structure of HPV16 E2 TAD (25) as a search model, where there is 36% sequence identity between BPV E2 and the HPV E2 TAD segment used (residues 1–188). Refinement was performed using REFMAC (26) and model rebuilding was carried out using X-Autofit (27) implemented in Quanta (Accelrys). Statistics of the X-ray data and final refined models are shown in Table 1.

Oxidative cross-linking and protein analysis

E2 TAD proteins were incubated at 1 mg ml^{-1} (4°C for 14–16 h) in 20 mM Tris–HCl pH 8.0, 0.15 M NaCl, 5% v/v glycerol, 0.01% NP40, 0.1 mM PMSF) with 20 or 0.05 mM DTT after buffer exchange with a G25 microspin column (Amersham Bioscience). Proteins were treated with 30 mM *N*-ethylmaleimide (NEM, from a 200 mM stock in ethanol) for 10 min at room temperature before heating to 95°C (5 min) and loading on a standard SDS–PAGE gel (12%, 29:1 acrylamide:*bis*-acrylamide). Full length E2 proteins were analysed on 8% gels (29:1 acrylamide:*bis*-acrylamide). Analytical gel filtration was performed on a Superdex 75 column (Amersham Bioscience). Gradient sedimentation of E2 (120–150 μg) was performed on 20–40% glycerol gradients spun for 16 h at 237 000 × g, at 4°C (Beckmann SW55 rotor). The buffer was as described earlier, except 100 mM NaCl. Sedimentation profiles were analysed by SDS–PAGE, after treating protein samples with *N*-ethylmaleimide as described

Table 1. Data collection and refinement statistics

Data collection		
Structure	Wild type	R172A mutant
Space group	$P6_122$	$P3_2$
Unit cell parameters (Å)	$a = 61.5$, $c = 236.3$	$a = 60.5$, $c = 89.4$
ESRF beamline	ID14-1	BM14
Wavelength (Å)	0.934	0.919
Resolution range, overall (Å)[a]	25.0–2.8	25.0–2.35
Number of unique reflections	7171 (620)	14352 (1259)
Redundancy[b]	7.3 (5.8)	1.9 (1.8)
Completeness (%)	99.2 (92.1)	93.3 (90.2)
Reflections with $I > 3\sigma_I$ (%)	83.6 (47.4)	83.3 (41.6)
$\langle I/\sigma_I \rangle$[c]	32.0 (3.5)	10.7 (2.5)
R_{merge}[c]	0.058 (0.495)	0.068 (0.325)
B-factor from Wilson plot (Å^2)	76.6	71.9
Refinement and model correlation		
Number of atoms	1595	1702
Number of reflections used in refinement	6594	13546
R-factor[d]	0.233	0.210
Number of reflections used for R_{free}	500	716
R_{free}[d]	0.281	0.241
Average B-factors		
Protein atoms (Å^2)	78.0	71.8
Solvent (Å^2)	75.9	77.4
Deviations from ideal geometry[e]:		
Bond distance (Å)	0.007 (0.020)	0.010 (0.020)
Angles (°)	1.0 (1.9)	1.1 (1.9)

[a]Values in brackets correspond to the outer resolution shell.
[b]The average number of observations of the same reflection.
[c]The value of the merging *R*-factor between equivalent measurements of the same reflection, $R_{merge} = (\Sigma\Sigma|I_j(hkl) - \langle I/(hkl)\rangle|)/(\Sigma\Sigma\langle I/(hkl)\rangle)$.
[d]Crystallographic *R*-factor, $R_{free} = \Sigma||F_o| - |F_c||/\Sigma|F_o|$.
[e]R.m.s. deviation from the standard values are given with target values in parentheses.

earlier, and densitometry (digitized images, Kodak 1D 3.5.4 software).

GST 'pulldown' assay

GST-E1 was purified as previously described (22). GST was purified on glutathione-sepharose followed by gel filtration. Ten pmol of GST-E1 or GST were bound to 10 μl of glutathione-sepharose before washing and binding of 1 pmol of E2 in 200 μl reaction (20 mM NaPhosphate pH 7.2, 135 mM NaCl, 10% glycerol, 0.1% NP40, 0.1 mg ml^{-1} BSA, 1 mM PMSF and 1 mM DTT) for 30 min. PKA-tagged E2 proteins (MG**RRAS**VH) were labelled using PKA (Novagen) and [^{32}P]γATP, and free ATP was removed using a G25 column. Binding reactions were washed in binding buffer, and recovered proteins analysed by SDS–PAGE after treatment with NEM. Gels were analysed by phosphorimaging (Fuji FLA3000, image guage V3.3 software).

DNA-binding reactions

Probes and binding reactions with E1 and E2 have been described before (8). Briefly, the BPV *ori* sequence cloned into the pUC19 vector is **TCACCGAAACCGGT**AAGTA AAGACTATGTATTTTTTCCCAGTGAATA<u>ATTGTT GTTAACAATAAT</u>CACA**CCATCACCGTT**, the distal (BS11) and proximal (BS12) E2 binding sites are shown in bold and the E1 BS underlined. The sequence of the

GCN4 binding site that replaces distal BS 11 is ATGACTCAT. Reactions that assayed E1E2–*ori* formation were performed in the absence of ATP, while reactions that assayed stimulation of E1–*ori* formation by GCN4E2 from a distal binding site contained 5 mM ATP (8,9). The E2BS9 probe was made by annealing two oligonucleotides, CCGGGAAGT**ACCGTTGCCGGT**CG AAC and CCGGGTTCG**ACCGGCAACGGT**ACTTC, and labelling with $[\alpha^{32}P]dCTP$ using Klenow exo⁻ (NEB), followed by a chase with 40 μM dCTP/dGTP. Gels were exposed to phosphorimager screens. E2 binding reactions were analysed on 6% (29:1 acrylamide:*bis*-acrylamide) gels and E1E2–*ori*-binding reactions on 5% (79:1 acrylamide:*bis*-acrylamide gels), both with 0.25 × TBE buffer. E1–*ori* complexes were resolved on agarose gels (1% TAE running buffer), after cross-linking with glutaraldehyde. Potassium permanganate footprinting was performed as described (9).

RESULTS

Crystal structure of the BPV E2 TAD reveals redox-dependent dimerization

We determined the crystal structure of the BPV TAD at 2.8 Å resolution. Notably, the crystals formed only in the absence of DTT. In the structure, two L-shaped monomers of the TAD are arranged in a manner resembling a handshake to form a dimer stabilized by a disulphide bond formed between Cys57 residues of the two monomers, Figure 1B. The dimer has overall dimensions of $45 \times 60 \times 65$ Å, and a substantial ~2500 Å² of surface area buried per monomer. Two contact areas of roughly equal size form, one between the N-terminal halves (N1) where the disulphide linkage resides and another between the C-terminal halves (N2) of two TADs. A pair of hydrogen bonds is formed in N1, between the side chains of Gln12 and Arg58 (not shown), and an ion pair is formed in N2 by the side chains of Arg172 and Asp175, circled and shown on the right of Figure 1B. The total number of direct inter-subunit hydrogen bonds, 2.4/1000 Å², is significantly lower than the average value of 7/1000 Å² of contact area observed in dimeric proteins (28), notwithstanding the more polar interface of E2, with 44% of interface atoms polar compared to the average value of 35% observed in stable dimers. Thus, the dimer appears to be largely stabilized by the disulphide linkage between the two monomers.

We also obtained crystals for R172A mutant TAD under the same conditions but with 2 mM DTT and solved the structure to 2.35 Å resolution. The crystals belong to the space group P3₂ with one molecule per asymmetric unit, inconsistent with any oligomeric arrangement. Comparison of the R172A structure with the structure of the wild-type protein shows that the mutant has an identical fold with the overall r.m.s. difference of 0.76 Å calculated over the Cα atoms. Most significant differences are in a few surface loops that adapt to new crystal contacts (Figure 1C). The data indicate that the inability of R172A to form the dimer is exclusively due to the reducing conditions and the R172A substitution.
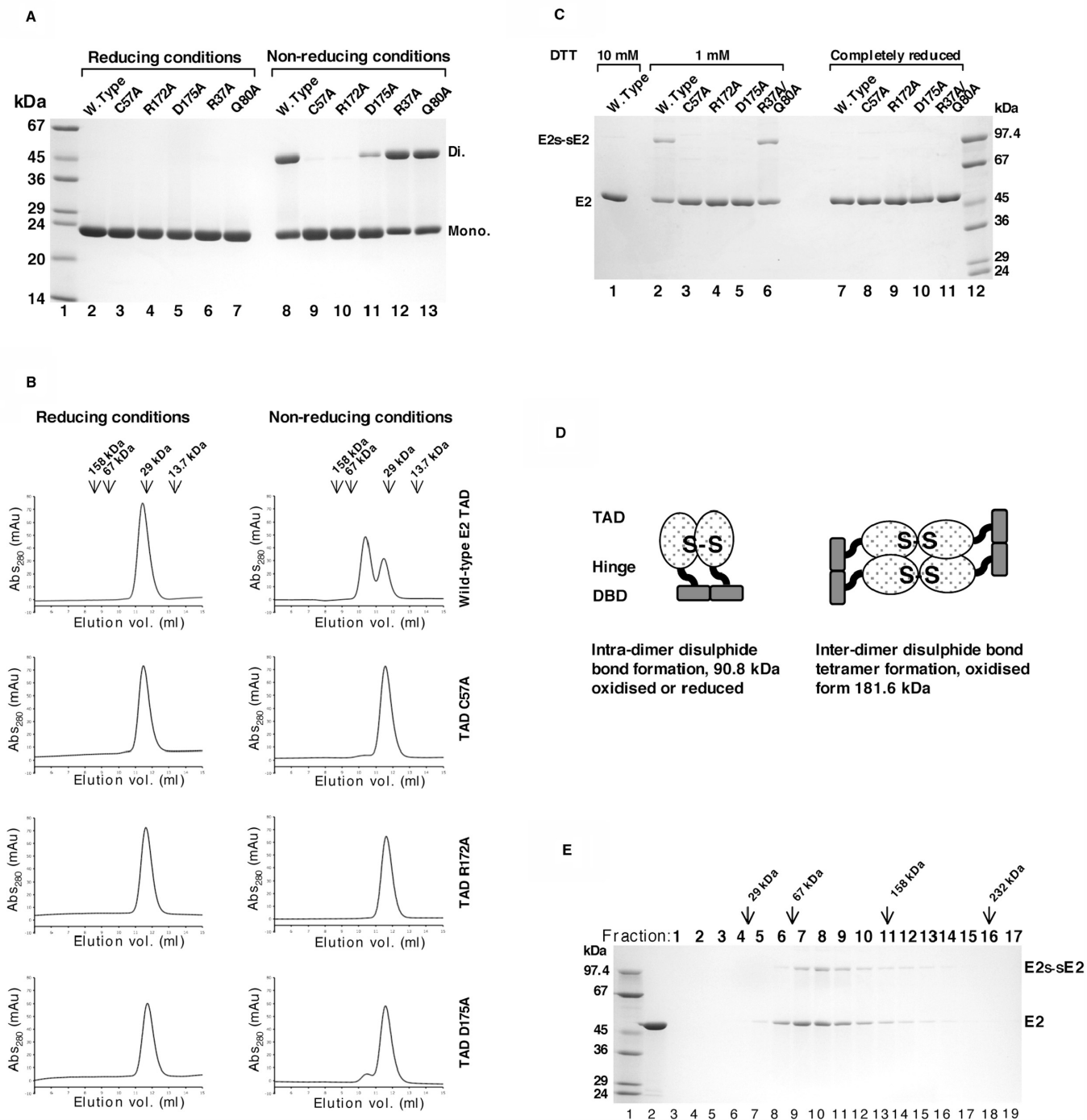
Redox-dependent dimerization of the BPV E2 TAD in solution

To determine if the E2 TAD dimer forms in solution Cys57 was exploited as a natural cross-linking group. Recombinant C57A, R172A and D175A substituted proteins were purified from *E. coli*. As negative controls we mutated residues R37 and Q80, involved in formation of the different HPV16 E2 TAD dimerization interface (25), to alanine. The CD spectra of all mutant proteins tested were similar to wild-type, demonstrating that their overall protein fold was conserved (not shown). In SDS–PAGE, all proteins were monomeric (23.86 kDa), under reducing conditions (20 mM DTT, Figure 2A). However, when the wild-type protein was incubated under non-reducing conditions (50 μM DTT), and treated with *N*-ethylmaleimide (NEM) to alkylate-free cysteine residues prior to electrophoresis, a dimer formed (lane 8). C57A and R172A were almost completely impaired for dimer formation, while D175A was significantly dimerization defective. R37A and Q80A behaved like wild-type, as did a double mutant R37A/Q80A (not shown). Dimerization under native conditions was confirmed by gel filtration. The wild-type TAD was monomeric under reducing conditions, but a dimeric peak formed under non-reducing conditions (Figure 2B top left and right). C57A, R172A and D175A mutant proteins eluted as a monomer under reducing or non-reducing conditions, except D175A where a small proportion of dimer was evident under non-reducing conditions, as in Figure 2A, lane 11. The dependence of stable dimerization on C57 cross-linking is consistent with the paucity of direct hydrogen bonds at the dimer interface (Figure 1B). Furthermore, there are other cysteine residues on the surface of the protein that have their side chains exposed, such as C5 and C160. However, these two cysteines do not result in TAD cross-linking under non-reducing conditions. These data therefore support the crystallographic data demonstrating the importance of Cys57 in domain N1 and residues R172 and D175 in N2 for specific dimer formation.

TADs dimerize within a pre-formed E2 dimer

To confirm redox-dependent dimerization in full length E2, E2 and mutants were purified by ion-exchange chromatography followed by gel filtration in 10 or 1 mM DTT and assayed for dimerization by SDS–PAGE after NEM treatment (Figure 2C). With 10 mM DTT, wild-type E2 was monomeric under denaturing conditions (lane 1). However, in the presence of 1 mM DTT a significant proportion of the protein formed cross-linked dimers (lane 2), that were dependent on Cys57 (lane 3). E2 R172A and D175A were also defective for redox-dependent dimerization (lanes 4 and 5), but not the double mutant R37A/Q80A (lane 6).

E2 forms stable dimers via the C-terminal DBD. The TAD interaction could occur either within a pre-formed dimer or between two E2 dimers, resulting in native molecular masses of ~90.8 and 181.6 kDa, respectively, as illustrated in Figure 2D. When glycerol gradient sedimentation followed by SDS–PAGE was performed in the presence of 1 mM DTT, Figure 2E, we only observed

Figure 2. Redox-dependent dimerization of the E2 TAD in solution. (**A**) Wild-type TAD and mutant proteins (15 μg, 0.4 mg ml^{-1}) were incubated under reducing (20 mM DTT) and non-reducing (50 μM DTT) conditions before treatment with *N*-ethylmaleimide and analysis by SDS–PAGE. (**B**) Gel-filtration analysis of the wild-type E2 TAD and mutants (100 μg, 1 mg ml^{-1}) with 10 or 0.05 mM DTT. The column was calibrated with the markers indicated. (**C**) Redox-dependent dimerization of full length E2 and mutants purified in 10 or 1 mM DTT and analysed by SDS–PAGE after treatment with NEM (8 μg each). 350 mM 2-mercaptoethanol was used to completely reduce samples. (**D**) Schematic showing intra- or inter-TAD dimerization. (**E**) Glycerol gradient sedimentation of E2 (1 mM DTT). Lane 1, marker and lane 2, E2 reduced.

protein peaks between the 67 and 158 kDa markers, and an overall sedimentation profile that was similar to the protein assayed in 10 mM DTT (data not shown). The sedimentation profiles of the reduced and oxidized forms

of E2 were almost coincidental, with native masses of 84 and 94 kDa, respectively. This difference is inconsistent with tetramer formation, demonstrating that the TAD–TAD interaction is intra-dimeric.

Oxidative TAD dimerization abolishes the E1–E2 protein–protein interaction

Comparison of the TAD dimer with the structure of the HPV E1–E2 complex (6), predicts that TAD dimerization would interfere with the E1–E2 interaction for two reasons, as illustrated in Figure 3A. First, TAD dimerization buries more than half of the protein surface area used in the E1–E2 interaction. Secondly, E2 TAD dimerization would prevent its interaction with E1, as E1 occupies the same space as residue segments 4–12 and 30–81 of the second E2 subunit within the E2 TAD dimer, as shown on Figure 3A. Here, the TAD subunit in blue is interacting with E1, while the subunit in red is seen to overlap with E1 (yellow surface). To test this we purified, in the presence of 1 mM DTT, E2 and E2 C57A that were tagged with a protein kinase A (PKA) recognition sequence for ^{32}P-labelling and used them in GST-pulldown assays. Figure 3B lane 1 shows input wild-type protein (E2s-sE2 dimer and E2 indicated). Only the non-cross-linked form of E2 bound GST-E1 immobilized on glutathione Sepharose (lane 2), while the C57A mutant retained full functionality in the E1 binding assay (lane 5). The proteins did not bind to GST alone (lanes 3 and 6). The BPV E1–E2 protein–protein interaction can therefore be effectively redox regulated.

DNA binding by oxidized E2

When binding of E2 to a high-affinity site was analysed by gel-shift assay, after equilibrating proteins in high (10 mM) or low (0.6 mM) DTT (Figure 4A), ∼70% of the complex that formed with wild-type E2 moved with increased mobility in the gel ([S-S]E2-DNA, lanes 5–7), compared to high DTT conditions (lanes 2–4). This form likely represents the internally cross-linked species, as it did not form with C57A, R172A (lanes 8–13) or D175A (not shown). Since the difference in charge and mass between the E2-DNA and [S-S]E2-DNA species is minimal, a probable explanation for the difference in gel-mobility is a change in molecular shape. This is consistent with the observation that the [S-S]E2 protein sediments at a slightly slower rate than the reduced species in glycerol gradient sedimentation experiments (Figure 2E), as would be predicted for a more compact spherical structure. Probe binding was also reduced by 30–40%, since E2 DNA binding is itself redox sensitive (14). We next asked if the oxidative effects on E2 DNA binding are reversible. As shown in Figure 4B, when E2 was pre-incubated at very low DTT concentration (<25 µM), DNA binding was abolished (lane 3 compared to 2, 10 mM DTT), but could be restored by supplementing binding reactions with increasing concentrations of DTT (lanes 4–7). DNA-binding activity was first recovered in the form of the cross-linked TAD dimer ([S-S]E2-DNA, not seen with C57A, lanes 10–13), which was converted to the non-cross-linked form at higher DTT concentrations. Together with the results in Figure 4A, these experiments demonstrate that Cys57 is a reversible and more reactive redox centre than C340 in the DBD (14).
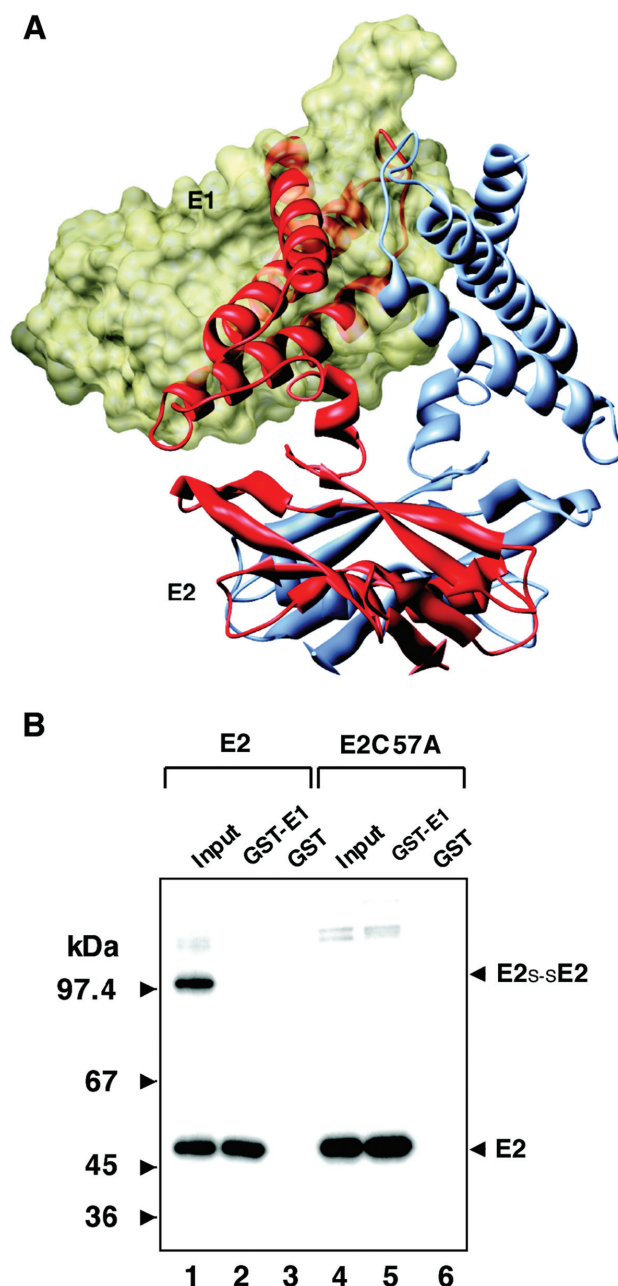
Figure 3. The E2–E2 TAD interaction interferes with the E1–E2 interaction. (**A**) The BPV E2 dimer is shown as a ribbon, in the same orientation and colours as in Figure 1B. The subunit shown in blue was overlapped with HPV18 E2 molecule of the E1–E2 complex (6). The HPV E1 monomer in the E1–E2 complex is represented as a semi-transparent molecular surface (yellow). A part of each of the three N-terminal helices of the red subunit of E2 overlap directly with the E1 molecule, as is illustrated by a blurring of the helices in red. The figure was generated using the program Chimera (40). (**B**) E2 and E2 C57A GST-pulldown assay. Twenty-five percent of input protein is compared to 50% recovery.
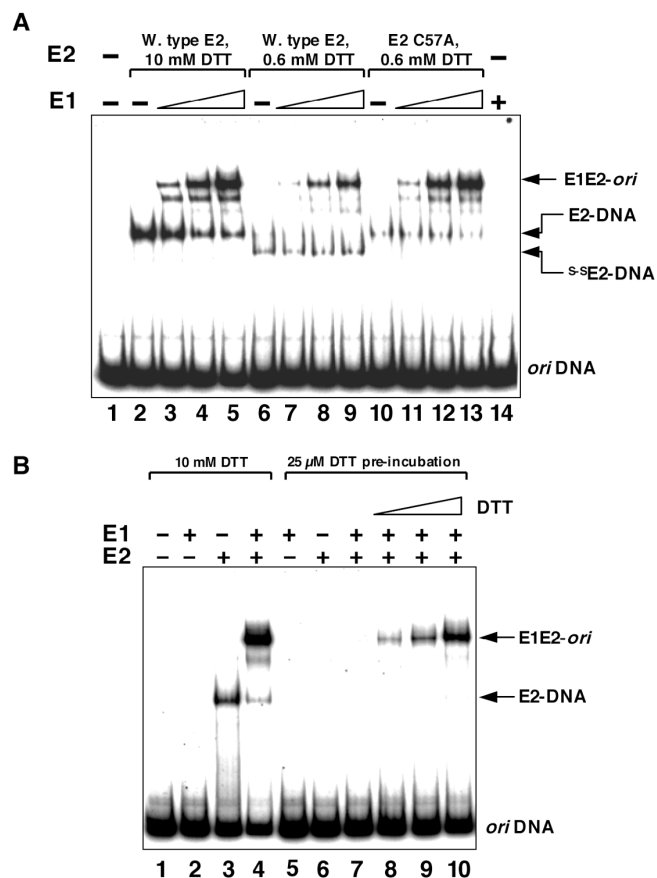
Oxidative TAD dimerization inhibits E1E2–*ori* pre-initiation complex formation

E1E2–*ori* formation was then analysed by gel-shift using an *ori* probe (Figure 1A), with the E1 binding site and E2 BS12, under reducing conditions (10 mM DTT) and low
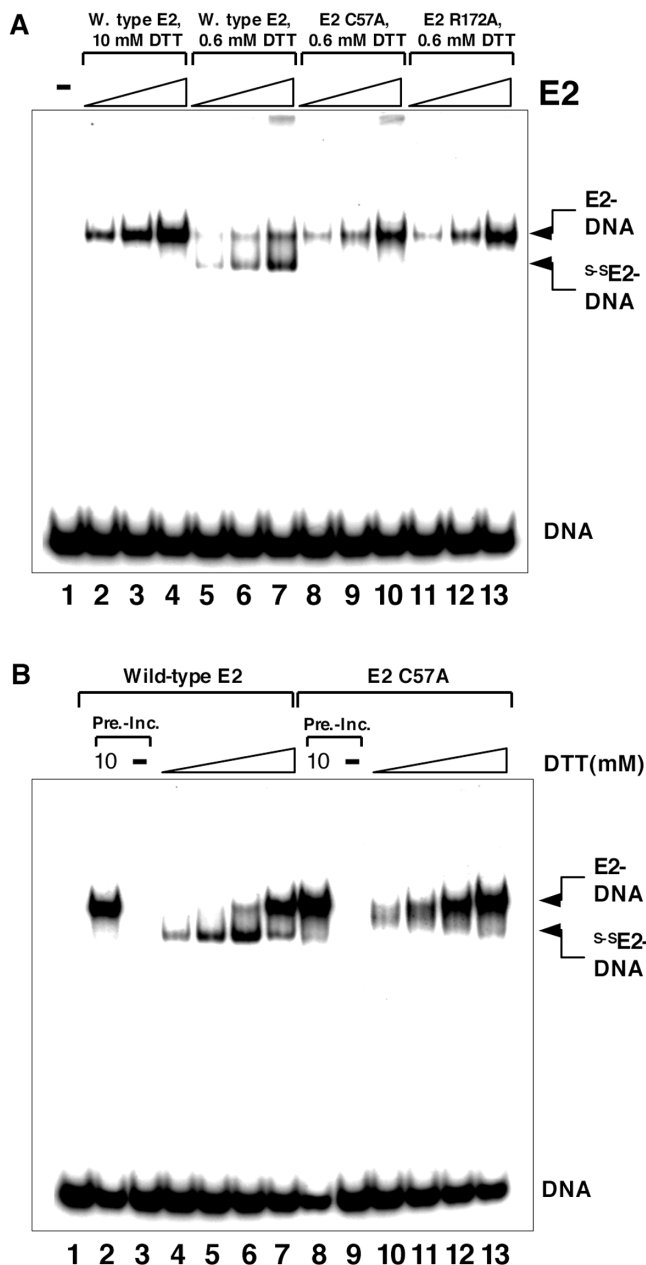
Figure 4. Redox-dependent E2-DNA binding. (**A**) Gel-shift analysis of wild-type E2, C57A and R172A (0.5–2 nM) binding to a high-affinity binding site, with 10 or 0.6 mM DTT. Cys57 cross-linking generates a high-mobility DNA–protein complex. (**B**) Reversal of DNA-binding inhibition and C57 cross-linking by DTT. Proteins were pre-incubated in 25 μM DTT and binding reactions (20 min incubation) supplemented with 0, 0.2, 0.4, 1 or 10 mM DTT. Lanes 2 and 8, control reactions maintained at 10 mM DTT. For wild-type E2, DNA-binding activity is first recovered in the form of the TAD cross-linked species (lanes 4–8), not seen with the C57A mutant (lanes 10–13).

Figure 5. Oxidative TAD dimerization and E1E2–*ori* pre-initiation complex formation (**A**) E1E2–*ori* formation assayed on a BPV *ori* probe with the E1 BS and E2 BS12 (0.05 nM; E2, 0.25 nM and E1 from 0.1 to 0.5 nM). E1E2–*ori* forms efficiently with wild-type E2 at 10 mM DTT (lanes 3–5) or with the C57A mutant (lanes 11–13). The $^{s\text{-}s}$E2–DNA complex does not form an E1E2–*ori* complex (lanes 6–9), and E1E2–*ori* complex formation is impaired with wild-type E2 at low DTT concentrations. (**B**) Recovery of E1E2–*ori* formation after oxidation of E2. Lanes 1–4, control reactions demonstrating E1E2–*ori* formation at 10 mM DTT. Lanes 5 and 6, E1 or E2 incubated alone with probe at 25 μM DTT. Lanes 7–10, 25 μM DTT pre-incubation and binding reactions supplemented with no additional DTT, 0.4, 1 or 10 mM DTT.

DTT conditions (0.6 mM). E2 DNA binding is itself redox sensitive and DNA binding is abolished at very low DTT concentrations. At 0.6 mM DTT, sufficient DNA-binding activity is retained, while ~70% of the observed E2 binding activity is in the form of the fast migrating $^{s\text{-}s}$E2-DNA species, as described earlier (Figure 4A and B).

With 10 mM DTT wild-type E2 bound DNA (Figure 5A, lane 2). When the concentration of E1 was increased, the E1E2–*ori* complex formed and the amount of detectable E2–DNA complex diminished (compare lanes 2–5). The minor species migrating between the E2 and E1E2–*ori* band shifts most probably correspond to intermediates in the E1–E2 assembly. With low DTT concentrations (0.6 mM), consistent with the results described in Figure 4A, a mixture of complexes corresponding to the oxidized and reduced forms of E2 formed (E2–DNA and $^{s\text{-}s}$E2–DNA, lane 6), but only the non-cross-linked form (E2–DNA) was observed with C57A (compare lanes 6 and 10). However, in the presence of E1 at low DTT concentrations significant differences were observed between wild-type E2 and C57A: with wild-type E2 formation of E1E2–*ori* was reduced compared to C57A (lanes 7–9, compared to 11–13),

while the E2-DNA-binding activity appeared similar for both proteins (lane 6 compared to 10). When the products of E2-DNA binding in these reactions are also compared, it is clear that for the wild-type protein (0.6 mM DTT) the amount of $^{\text{S-S}}$E2DNA complex that forms does not change when E1 is added (lanes 7–9 compared to 11–13), but the amount of non-cross-linked complex (E2-DNA) diminishes. Comparing the ratios of the E2 to E1E2–*ori* band-shifts indicate that conditions that favour $^{\text{s-s}}$E2–DNA complex formation are inhibitory for E1E2–*ori* formation. Furthermore, E2 C57A assayed in 0.6 mM DTT was as competent as the wild-type protein assayed at high DTT concentration for E1E2–*ori* formation (lanes 3–5 compared to 11–13), suggesting that the redox-dependent change in E2-DNA-binding affinity has a minimal effect on E1 recruitment to *ori*. This is consistent with the E2 TAD–E1 HD interaction being a major component of cooperative E1–E2 DNA binding (6). E1 does not bind the probe without E2 (lane 14), and E1 *ori* binding alone is relatively insensitive to DTT concentration over the range tested (10 to 0.05 mM, see later). We next asked if E1E2–*ori* formation could be restored after complete oxidation of the proteins. The results shown in Figure 5B demonstrate that pre-incubation in 25 µM DTT abolishes E2-DNA binding (lane 6 compared to 3, as demonstrated in Figure 4B) and E1E2–*ori* complex formation (lane 7 compared to 4). However, supplementing binding reactions with increasing concentrations of DTT restored E1E2–*ori* complex formation (lanes 8–10), indicating that the proteins are not intrinsically susceptible to irreversible oxidative inactivation. Our biochemical studies therefore demonstrated that C57-dependent oxidative dimerization of the E2 TAD, within a stable E2 dimer otherwise dimerized by the tight DBD interaction (21), can regulate E1 recruitment to *ori*, the first event in replication initiation.

Oxidative TAD dimerization suppresses E2-dependent formation of an E1 replication initiation complex

In BPV a second high-affinity E2 binding site (E2 BS11) is positioned 33 bp upstream of the E1–E2 BS12 binding site arrangement, as depicted in Figure 1A. A distal E2 site alone can drive replication in transient assays (3), from an E1E2–*ori*-like complex (10). However, its most likely role in viral replication is to promote formation of a replication active *ori*-melting complex from the primary E1–*ori* complex derived from E1E2–*ori* (9). In the experiments described earlier in Figure 5A, a direct assessment of the effects of TAD cross-linking on E1E2–*ori* pre-initiator complex formation is complicated by the redox-sensitive DNA-binding component of E2. However, it has been demonstrated that when E2 functions from a distal position, there is no requirement for the E2 DBD, in marked contrast to initiator complex assembly from proximal BS12 where there is an obligatory requirement for a specific E1 DBD–E2 DBD interaction (29). In the former case, targeting of the E2 TAD to DNA can be achieved with a heterologous DBD, and a chimaeric E2 protein where the E2 DBD is replaced with that of the yeast transcription factor GCN4 (GCN4E2) is active in

transient replication assays (29). Since DNA binding of GCN4 is not redox-sensitive, we were able to test directly the effect of oxidative TAD dimerization on formation of an active E1–*ori* initiator complex. Accordingly, reactions were assembled with purified recombinant E1, E2GCN4 and a template with a distal GCN4 binding site, with the ATP (5 mM) required for formation of an E1–*ori* DNA melting complex. Stimulation of E1–*ori* complex formation by GCN4E2 proteins was measured by gel-shift analysis, and *ori*-DNA melting with the potassium permanganate footprinting assay.

In Figure 6A, purified GCN4E2 (GE2) and the C57A mutant (GE2C57A) were assayed in parallel for E1–*ori* complex formation and DNA melting under reducing conditions (2 mM DTT). The results of the gel-shift assay are shown above the results of the potassium permanganate assay; the lane numbers in each case correspond to the same reaction. In the gel-shift shown earlier (Figure 6A), GCN4E2 and the C57A mutant demonstrated little difference in their ability to promote E1–*ori* complex formation at low E1 concentration (lanes 5–8 and 10–13 compared to lane 4 with E1 alone). Likewise, in the potassium permanganate assay shown below, both proteins promoted *ori*-melting to similar extents, over the A/T-rich region and in the proximal E2 BS (lanes 5–8 and 10–13 compared to lane 4). However, we note that high concentrations of the chimaeric proteins appeared inhibitory for melting, which is not normally observed with wild-type E2 (8,9). At low DTT concentrations (0.05 mM), Figure 6B, wild-type GCN4E2 was significantly impaired in its ability to stimulate E1 complex formation (lanes 5–8 and 10–13 compared to 4), while the C57A mutant functioned like the proteins assayed at 2 mM DTT. The impaired ability of wild-type to stimulate E1–*ori* complex formation was reflected in the potassium permanganate melting assay, shown below. Here, the extent of *ori*-melting promoted by the highest concentrations of GCN4E2 was comparable to those observed at the lowest concentrations of the C57A mutant (lanes 8 and 10). Oxidative TAD dimerization therefore impinges on all levels of E2-dependent replication initiation complex assembly.

DISCUSSION

We have characterized structurally and functionally a dimeric form of the BPV E2 transactivation domain. A remarkable feature of this novel BPV E2 TAD dimer is that it is stabilized by only a few direct inter-subunit hydrogen-bonding interactions and a salt bridge resulting in a relatively loose contact. However, under non-reducing conditions the two subunits covalently cross-link by a reversible disulphide bond, thus stabilizing the dimer interface. In a pre-formed E2 dimer stabilized via the tight interaction of the DBDs, two TAD domains linked via flexible hinges are always in close proximity. The flexible or 'open' nature of the TAD interface would allow the interaction with regulatory partners, but upon disulphide bond formation a 'closed' dimeric form with reduced surface area for contact would result. This type of post-translational modification is reminiscent of the
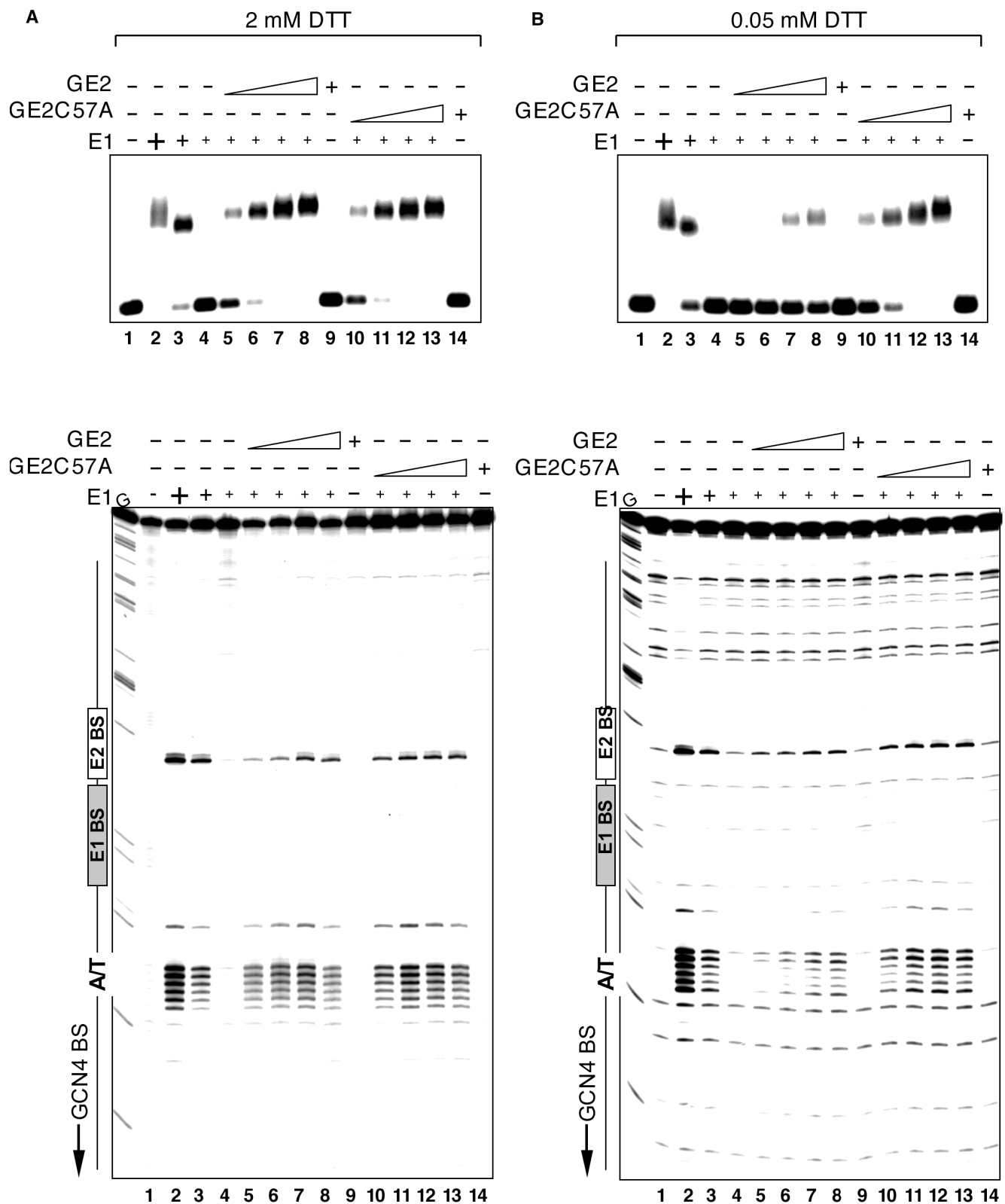
Figure 6. Replication initiation complex formation and *ori*-melting under reducing and non-reducing conditions. (**A**) Stimulation of an E1–*ori*-melting complex formation by wild-type GCN4E2 (E2 amino acids 1–319 fused to GCN4 amino acids 218–282) and C57A mutant under reducing conditions (2 mM DTT). Binding reactions were assembled and a proportion of the reaction mix analysed for site occupancy by gel-shift (above) and for *ori*-melting by KMnO$_4$ footprinting (below). The probe contained a GCN4 binding site at a distal position, replacing E2 BS11. Lane 1, free probe. Lanes 2–4, E1 alone, 50, 25 and 10 nM. Lanes 5–8, 10 nM E1 and 0.375, 0.75, 1.5 and 3 nM wild-type GCN4E2 (GE2). Lane 9, 3 nM GCN4E2. Lanes 10–14, as 5–9 but containing the C57A TAD mutant (GE2C57A). (**B**) Proteins assayed under non-reducing conditions, 0.05 mM DTT. All reactions were otherwise as described in (A).
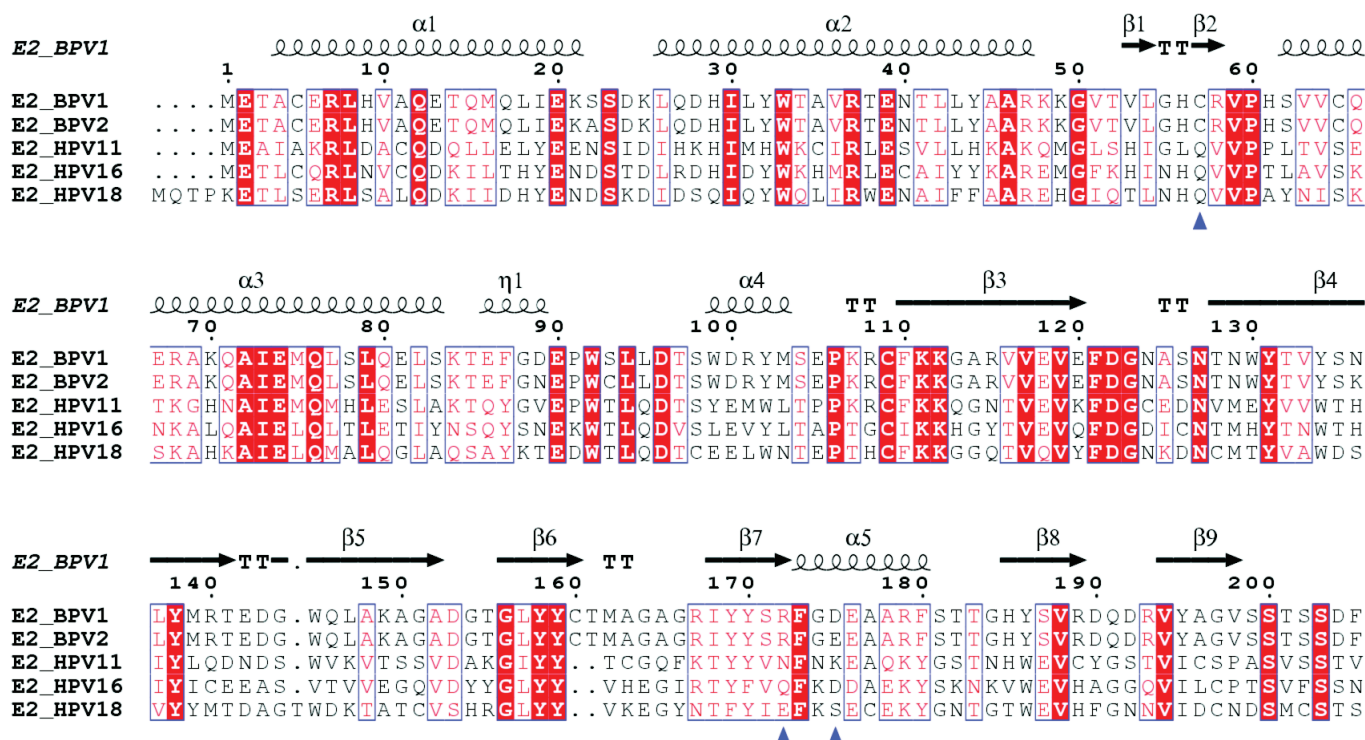
Figure 7. Alignment of E2 TAD sequences from BPV1, BPV2, HPV11, HPV16 and HPV18 generated by ESPript (41) with the secondary structure of BPV 1 TAD shown above. Residues that stabilize the dimer and that were mutated in this study are indicated with the blue triangles.

modes of regulation of the redox sensors Yap1 (30) and OxyR (31) that function in micro-organisms to regulate the response to environmental redox changes. This structure therefore has the hallmarks of a regulatory sulphydryl switch.

It is noteworthy that the BPV TAD dimer is distinctly different in its contacts from those seen in the HPV 16 E2 TAD (25), and that in HPV 11 the species is apparently monomeric (32). However, at the amino-acid level TAD sequences exhibit a great degree of variability (2), with only 32, 33 and 36% sequence identity between BPV E2 TAD and the corresponding domains in HPV18, HPV16 and HPV 11, respectively (Figure 7). Examination of the amino-acid sequences of E2 proteins from various PVs does show that a cysteine at position 57 is found in BPV type 1 and 2 that cause skin warts in cattle. Other papillomaviruses with known sequence do not have a cysteine in the equivalent position, indicating that the disulphide bond observed in BPV will not form and that replication control will not be achieved using an identical redox sensor to the one we describe. However, it is possible that similar dimers can form in other PVs but are stabilized by different post-translational events. It is also possible that the varying types of oligomerization observed in PV E2 structures reflect the somewhat different regulatory roles played by E2 in the various viral sub-groups. For example, the arrangement of E1 and E2 binding sites in a tandem array at *ori* (Figure 1A) is unique to the fibropapillomaviruses, and the significance of the E1E2–*ori* complex that therefore forms is not clear. These viruses also generate distinctive lesions that have a fibroblastic as well as epithelial component, and are large

with a high viral burden characteristic of vigorous replication. The Cys57-induced dimerization of E2 in BPV may thus reflect host-specific adaptation of the virus selected by evolution against other modifications.

Our findings suggest that oxidative TAD dimerization could have a role in controlling BPV replication initiation by masking and unmasking a binding surface for interaction with the initiator protein E1. E2 may act as a redox sensor where determinants in the TAD and DBD regulate initiator complex assembly, as modelled in Figure 8. In Figures 3B, 5A and 6 we demonstrate that disulphide bond formation abolishes the E1–E2 protein–protein interaction and replication initiation complex formation *in vitro*, consistent with the structural analysis of the E1E2 complex (6). Furthermore, we demonstrate in Figure 4 that Cys57 is a more sensitive redox centre than Cys340, the accepted determinant of redox-dependent E2-DNA binding (14). This therefore implies a significant role for TAD dimerization in regulating BPV E2 activity. The intracellular redox potential is known to fluctuate in the cell-cycle, with a pro-oxidative state being established at the G1/S boundary, which lasts until mitosis (18,33,34). Furthermore, cell-cycle arrest during oxidative stress may be through a Cdc25C redox response (35). It has therefore been hypothesized that critical cell-cycle events are regulated by redox switches (33), and our data on BPV E1/E2 proteins provides experimental evidence indicating that replication initiation reactions may be under such control. S-phase replication of BPV occurs by a 'random choice' mechanism rather than each replicon replicating only once (36). The redox mechanism of control is not necessarily inconsistent with the random
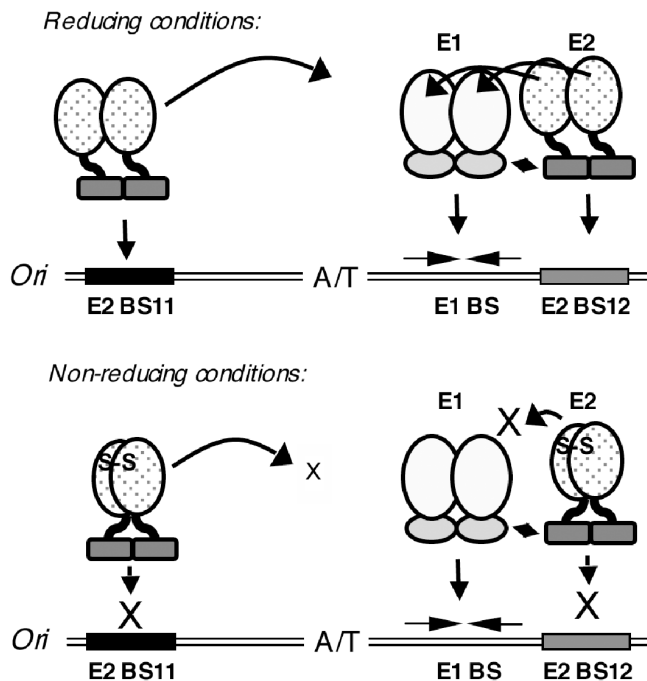
Figure 8. A model for control of BPV E1 initiator complex assembly with E2 as a redox sensor. The domain structures of E1 and E2 and *ori* is as depicted as in Figure 1A. Under reducing conditions the TAD dimerization through the disulphide bond does not occur, the E1 interaction surface is accessible for cooperative E1 binding and initiator complex assembly through proximal and distal E2 binding sites in *ori*. Under non-reducing conditions, disulphide bond formation between C57 residues in each TAD sub-domain stabilizes the TAD dimer, burying the principal E1 binding surface and thus preventing the E1–E2 interaction. Together with the reduction in E2-DNA binding affinity upon oxidation of C340 in the DBD, initiator complex assembly is compromised.

choice mode, since E1–E2 dissociation occurs on initiation (8) and would be required before TAD cross-linking could occur. In the pro-oxidative environment of S-phase E2 TAD cross-linking could prevent further initiation until E2 reduction restores the E1–E2 interaction. This mechanism may function, with the assistance of the redox control of E2-DNA binding (14) and cyclin-dependent kinase activity (37), as part of the licensing system that ensures the stable propagation of the BPV genome. Redox control may negatively regulate initiation, while cyclin activity provides an initiating signal confining replication to S-phase.

Papillomavirus transcription and replication are also both tightly coupled to epithelial differentiation. A gradient of protein oxidation exists across the dermis, with the stratum corneum exposed to an oxidative environment (38). In the outer layers of the dermis BPV switches from a Cairns-type to a rolling-circle mode of replication that may not require E2 (39). Oxidative inactivation of E2 could be the mechanism whereby replication changes from an E1–E2 regulated to an E1-only unregulated mode that drives high copy number viral amplification. The process of characterizing redox switches directly in cultured cells is inherently complex and has thus far not been achieved in mammalian cells, where the redox status of cells is difficult to measure,

control or correlate to the *in vivo* situation. A verification of our proposals therefore awaits the development of systems to achieve just this, and may reveal additional regulatory roles for E2 redox-dependent dimerization. However, our structure-function study with BPV should provoke renewed interest in this area, and may lead to the discovery of similar redox sensors that function in the mammalian cell-cycle or epithelial differentiation.

REFERENCES

1. zur Hausen,H. (1994) Molecular pathogenesis of cancer of the cervix and its causation by specific human papillomavirus types. *Curr. Top. Microbiol. Immunol.*, **186**, 131–156.
2. Giri,I. and Yaniv,M. (1988) Structural and mutational analysis of E2 *trans*-activating proteins of papillomaviruses reveals three distinct functional domains. *EMBO. J.*, **7**, 2823–2829.
3. Ustav,E., Ustav,M., Szymanski,P. and Stenlund,A. (1993) The bovine papillomavirus origin of replication requires a binding site for the E2 transcriptional activator. *Proc. Natl Acad. Sci. USA*, **90**, 898–902.
4. Thorner,L., Lim,D. and Botchan,M. (1993) DNA-binding domain of bovine papillomavirus type 1 E1 Helicase: structural and functional aspects. *J. Virol.*, **67**, 6000–6014.
5. Yasugi,T., Benson,J., Sakai,H., Vidal,M. and Howley,P. (1997) Mapping and characterisation of the interaction domains of human papillomavirus type 16 E1 and E2 proteins. *J. Virol.*, **71**, 891–899.
6. Abbate,E.A., Berger,J.M. and Botchan,M.R. (2004) The X-ray structure of the papillomavirus helicase in complex with its molecular matchmaker E2. *Genes Dev.*, **18**, 1981–1996.
7. Chen,G. and Stenlund,A. (1998) Characterisation of the DNA-binding domain of the bovine papillomavirus replication initiator E1. *J. Virol.*, **72**, 2567–2576.
8. Sanders,C. and Stenlund,A. (1998) Recruitment and loading of the E1 initiator protein: an ATP-dependent process catalysed by a transcription factor. *EMBO. J.*, **17**, 7044–7055.
9. Sanders,C. and Stenlund,A. (2000) Transcription factor loading of the E1 initiator reveals modular assembly of the papillomavirus origin melting complex. *J. Biol. Chem.*, **275**, 3522–3534.
10. Sanders,C. and Stenlund,A. (2001) Mechanism and requirements for bovine papillomavirus, type 1, E1 initiator complex assembly promoted by the E2 transcription factor bound to distal sites. *J. Biol. Chem.*, **276**, 23689–23699.
11. Abate,C., Patel,L., Rauscher,F.J.3rd and Curran,T. (1990) Redox regulation of fos and jun DNA-binding activity *in vitro*. *Science*, **249**, 1157–1161.
12. Matthews,J.R., Wakasugi,N., Virelizier,J.L., Yodoi,J. and Hay,R.T. (1992) Thioredoxin regulates the DNA binding activity of NF-kappa B by reduction of a disulphide bond involving cysteine 62. *Nucleic Acids Res.*, **20**, 3821–3830.
13. Wu,X., Bishopric,N.H., Discher,D.J., Murphy,B.J. and Webster,K.A. (1996) Physical and functional sensitivity of zinc

finger transcription factors to redox changes. *Mol. Cell. Biol.*, **16**, 1035–1046.

14. McBride,A., Klausner,R. and Howley,P. (1992) Conserved cysteine residue in the DNA-binding domain of the bovine papillomavirus type 1 E2 protein confers redox regulation of the DNA-binding activity *in vitro*. *Proc. Natl Acad. Sci. USA*, **89**, 7531–7535.

15. Shibanuma,M., Kuroki,T. and Nose,K. (1988) Induction of DNA replication and expression of proto-oncogenes c-*myc* and c-*fos* in quiescent balb/3T3 cells by xanthine-xanthine oxidase. *Oncogene*, **3**, 14–21.

16. Hockenbery,D., Oltvai,Z., Yin,Y., Milliman,C. and Korsmeyer,S. (1993) Bcl-2 functions in an antioxidant pathway to prevent apoptosis. *Cell*, **75**, 241–251.

17. de Haan,J.B., Cristiano,F., Iannello,R., Bladier,C., Kelner,M.J. and Kola,I. (1996) Elevation in the ratio of Cu/Zn superoxide dismutase to glutathione peroxidase activity induces features of cellular senescence and this effect is mediated by hydrogen peroxide. *Hum. Mol. Genet.*, **5**, 283–292.

18. Irani,K., Xia,Y., Zweier,J.L., Sollott,S.J., Der,C.J., Fearon,E.R., Sundaresan,M., Finkel,T. and Goldschmidt-Clermont,P.J. (1997) Mitogenic signalling mediated by oxidants in Ras-transformed fibroblasts. *Science*, **275**, 1649–1652.

19. Allen,R. and Balin,A. (1989) Oxidative influence in development and differentiation:an overview of free radical theory of development. *Free Radic. Biol. Med.*, **6**, 631–661.

20. Barford,D. (2004) The role of cysteine residues in redox sensitive regulatory switches. *Curr. Opin. Struct. Biol.*, **14**, 679–686.

21. Hegde,R.S., Grossman,S.R., Laimins,L.A. and Sigler,P.B. (1992) Crystal structure at 1.7 Å of the bovine papillomavirus-1 E2 DNA-binding domain bound to its DNA target. *Nature*, **359**, 505–512.

22. Sedman,T., Sedman,J. and Stenlund,A. (1997) Binding of the E1 and E2 proteins to the origin of replication of bovine papillomavirus. J. Virol., **71**, 2887–2896.

23. Otwinowski,Z. and Minor,W. (1997) Processing of X-ray diffraction data collected in oscillation mode. *Meth. Enzymol.*, **276**, 307–326.

24. CCP4. (1994) The CCP4 suite: programs for protein crystal-lography. *Acta Crystallog. Sect. D*, **50**, 760–763.

25. Antson,A.A., Burns,J.E., Moroz,O.V., Scott,D.J., Sanders,C.M., Bronstein,I.B., Dodson,G.G., Wilson,K.S. and Maitland,N.J. (2000) Structure of the intact transactivation domain of the human papillomavirus E2 protein. *Nature*, **403**, 805–809.

26. Murshudov,G., Vagin,A. and Dodson,E. (1997) Refinement of macromolecular structures by the maximum likelihood method. *Acta Crystallog. Sect. D*, **53**, 240–255.

27. Oldfield,T.J. (1996). Real space refinement as a tool for model building. In Dodson,E, Moore,M, Ralph,A and Bailey,S (eds), *Macromolecular Refinement. Proceedings of the CCP4 Study Weekend* Daresbury Laboratory, Warrington, UK, pp. 67–74.

28. Jones,S. and Thornton,J. (1996) Principles of protein-protein interactions. *Proc. Natl Acad. Sci. USA*, **93**, 13–20.

29. Berg,M. and Stenlund,A. (1997) Functional interactions between papillomavirus E1 and E2 proteins. *J. Virol.*, **71**, 3853–3863.

30. Wood,M., Storz,G. and Tjandra,N. (2004) Structural basis for redox regulation of Yap1 transcription factor localization. *Nature*, **430**, 917–921.

31. Choi,H.-J., Kim,S.-J., Mukhopadhyay,B., Cho,S., Woo,J.-R., Storz,G. and Ryu,S.-E. (2001) Structural basis of the redox switch in the OxyR transcription factor. *Cell*, **105**, 103–113.

32. Wang,Y., Coulombe,R., Cameron,D.R., Thauvette,L., Massariol,M.J., Amon,L.M., Fink,D., Titolo,S., Welchner,E. *et al.* (2004) Crystal structure of the E2 transactivation domain of human papillomavirus type 11 bound to a protein interaction inhibitor. *J. Biol. Chem.*, **279**, 6976–6985.

33. Menon,S.G., Sarsour,E.H., Spitz,D.R., Higashikubo,R., Sturm,M., Zhang,H. and Goswami,P.C. (2003) Redox regulation of the G_1 to S phase transition in the mouse embryo fibroblast cell cycle. *Cancer Res.*, **63**, 2109–2117.

34. Li,N. and Obery,T. (1998) Modulation of antioxidant enzymes, reactive oxygen species, and glutathione levels in mangansese superoxide dismutase overexpressing NIH/3T3 fibroblasts during the cell cycle. *J. Cell. Physiol.*, **177**, 148–160.

35. Savitsky,P. and Finkel,T. (2002) Redox regulation of Cdc25C. *J. Biol. Chem.*, **277**, 20535–20540.

36. Gilbert,D. and Cohen,S. (1987) Bovine papilloma virus plasmids replicate randomly in mouse fibroblasts throughout S phase of the cell cycle. *Cell*, **50**, 59–68.

37. Cueille,N., Nougarede,R., Mechali,F., Philippe,M. and Bonne-Andrea,C. (1998) Functional interaction between the bovine papillomavirus virus type 1 replicative helicase E1 and cyclin E-Cdk2. *J. Virol.*, **72**, 7255–7262.

38. Thiele,J.J., Hsieh,S.N., Briviba,K. and Sies,H. (1999) Protein oxidation of human stratum corneum: susceptibility of keratins to oxidation *in vitro* and presence of keratin oxidation gradients *in vitro*. *J. Invest. Dermatol.*, **113**, 335–339.

39. Burnett,S., Zabielski,J., Moreno-Lopez,J. and Pettersson,U. (1989) Evidence for multiple vegetative DNA replication origins and alternative replication mechanisms of bovine papillomavirus type 1. *J. Mol. Biol.*, **206**, 239–244.

40. Pettersen,E.F., Goddard,T.D., Huang,C.C., Couch,G.S., Greenblatt,D.M., Meng,E.C. and Ferrin,T.E. (2004) UCSF Chimera - a visualization system for exploratory research and analysis. *J. Comput. Chem.*, **25**, 1605–1612.

41. Gouet,P., Robert,X. and Courcelle,E. (2003) ESPript/ENDscript: extracting and rendering sequence and 3D information from atomic structures of proteins. *Nucleic Acids Res.*, **31**, 3320–3323.